ISSN 0021-3640, JETP Letters, 2022, Vol. 116, No. 11, pp. 804–816. © Pleiades Publishing, Inc., 2022.
Russian Text © The Author(s), 2022, published in Pis'ma v Zhurnal Eksperimental'noi i Teoreticheskoi Fiziki, 2022, Vol. 116, No. 11, pp. 779–792.

CONDENSED MATTER

Synthesis and Magnetic Properties of Iron Polyhydrides at Megabar Pressures

A. G. Gavriliuk[a, c, d, *], V. V. Struzhkin[b], S. N. Aksenov[a], A. G. Ivanova[a, c], A. A. Mironovich[a], I. A. Troyan[a, c, d], and I. S. Lyubutin[c]

[a] *Institute for Nuclear Research, Russian Academy of Sciences, Troitsk, Moscow, 108840 Russia*
[b] *Center for High Pressure Science and Technology Advanced Research (HPSTAR), Pudong, 201203 Shanghai, People's Republic of China*
[c] *Shubnikov Institute of Crystallography, Federal Scientific Research Centre Crystallography and Photonics, Russian Academy of Sciences, Moscow, 119333 Russia*
[d] *Immanuel Kant Baltic Federal University, Kaliningrad, 236041 Russia*
**e-mail: gavriliuk@mail.ru*

Received October 4, 2022; revised October 21, 2022; accepted October 21, 2022

Iron polyhydrides have been synthesized at pressures of 77–157 GPa and temperatures up to 2000 K by the laser heating of an iron–borazane (ammonia borane NH_3BH_3) sample in diamond anvil cells. X-ray spectra of the synthesized products indicate the formation of several FeH_x phases, in which (in two cells) reflections of FeH_2 iron hydride with the tetragonal $I4/mmm$ phase are reliably detected. The magnetic and electronic properties of FeH_x compounds have been studied by nuclear forward scattering spectroscopy on Fe-57 nuclei at high pressures in the temperature range of 4–300 K in external magnetic fields up to 5 T. The nuclear forward scattering data indicate at least seven FeH_x compounds with very different electronic and magnetic properties. The Néel temperature T_N determined for the FeH_2 phase at a pressure of 82 GPa is about 174 K. One of the striking results is the observation of the FeH_x phase remaining magnetically ordered at a pressure of 128 GPa in the entire temperature range of 4–300 K. Such a high pressure is characteristic of the boundary between the lower mantle and the outer core of the Earth. The existence of a magnetic phase of an iron compound at such a record high pressure is unique and has not yet been observed.

DOI: 10.1134/S0021364022602433

1. INTRODUCTION

Iron is one of the most abundant elements on the Earth. The fundamental electronic, magnetic, and structural properties of iron and its simple compounds are very important for understanding the structure of strongly correlated electron systems and for studying the properties of inner layers of the Earth. Iron polyhydrides are among possible materials in the mantle and the core of the Earth. Iron polyhydrides also allow the existence of superconducting phases belonging to the recently discovered new family of high-temperature superconductors—metal polyhydrides [1–3].

The discovery of superconductivity with the critical temperature T_c above 200 K in SH_3 [1, 2], LaH_{10} [3], and YH_6 [4] opened an era of high-temperature superconductors based on metal polyhydrides [5, 6]. From 2015 to date, the following metal polyhydrides with relatively high T_c values approaching room temperature have been synthesized (see reviews [5, 6]): PH_x with $T_c > 100$ K at 207 GPa, YH_x with $T_c = 243$ K above 200 GPa, ThH_x with $T_c = 161$ K below 175 GPa, PrH_x with $T_c = 9$ K below 130 GPa, $LaYH_x$ with $T_c = 253$ K below 183 GPa, CeH_x with $T_c = 115–120$ K below 95 GPa, SnH_x with $T_c = 70$ K below 200 GPa, BaH_x with $T_c \approx 20$ K below 140 GPa, CaH_x with $T_c = 215$ K at 172 GPa, ScH_x with $T_c = 22.4$ K at 156 GPa, and LuH_x with $T_c = 15$ K at 128 GPa.

It is also noteworthy that the chemical composition, the structure, and the electronic and magnetic properties of materials in the upper and lower mantles and the core of the Earth are still incompletely known. Iron is one of the key elements in the mantle and the core of the Earth. It is accepted that the core of the Earth consists primarily of iron with a minor addition of nickel, other predominantly light elements S, Si, and C, and hydrogen [7–10]. Iron is present in the mantle layers in the form of complex oxide compounds. Consequently, the study of the structure and magnetic and electronic properties of iron compounds, in particular, iron–hydrogen compounds, at high pressures is of great importance for the reconstruction of the structure of the inner spheres of the

Earth and for the understanding of their physical properties.

The most probable stable phases of iron hydrides were sought using ab initio density functional theory calculations with a plane wave basis and pseudopotentials [11, 12], USPEX evolutionary algorithm [13, 14], particle swarm optimization [15–17], and random search with use of the lattice dynamic method in the quasiharmonic approximation [18]. The authors of the cited works described the structures of iron hydrides with different compositions and calculated regions of their thermodynamic stability. Cubic FeH can exist up to 400 GPa [14, 18]. Hydride Fe_3H_5 (space group $P6_3/mmc$) is stable in the range of 50–145 GPa [14, 17], FeH_2 (space group $I4/mmm$) exists at 45–130 GPa [11, 14, 17], Fe_3H_8 (space group $Pm\text{-}3m$) is stable up to 75 GPa [14], and FeH_3 (space group $Pm\text{-}3m$) exists above 65 GPa [11, 14] up to 400 GPa [13]. According to calculations, FeH_4 can exist in the range of 100–240 GPa in the cubic (space group $P2_13$), orthorhombic (space group $Imma$), and monoclinic (space group $P2_1/m$) modifications [13, 15, 17]. The tetragonal Fe_3H_{13} and FeH_5 (space group $I4/mmm$) phases are stable in the range of 75–150 GPa [14]. The orthorhombic FeH_5 phase with the space group $Cmca$ is possible above 200 GPa [18]. The monoclinic (space group $C2/m$) and orthorhombic (space group $Cmmm$) modifications [14, 16] in the range of 35–115 GPa, as well as the monoclinic phase with the space group $C2/c$ above 200 GPa [16, 18], were predicted for FeH_6. Metastable FeH_7 and FeH_8 hydrides can exist in the pressure range of 150–300 GPa [16].

Recent theoretical studies predict superconductivity in the FeH_5 (space group $I4/mmm$) [12, 14, 19] and FeH_6 (space group $Cmmm$) iron hydrides with T_c up to 50 K at 130–150 GPa. However, the calculations reported in [20] exclude superconductivity in the FeH_5 phase and other iron hydrides.

The FeH iron hydride in the cubic [21] and hexagonal modifications [11, 22–24] and the predicted FeH_2, FeH_3, and FeH_5 phases have been experimentally obtained and examined [11, 12].

According to our recent nuclear forward scattering (NFS) studies of the Fe-57 isotope, pure iron is diamagnetic or paramagnetic with a very low magnetic moment in the pressure range of 13–241 GPa at temperatures of 4.2–300 K [25, 26]. Consequently, it can be assumed that the nonmagnetic FeH_x phases at pressures above the $\alpha \rightarrow \varepsilon$ transition (at a pressure of 13 GPa and room temperature) can be superconducting with a fairly high critical temperatures T_c.

According to theoretical predictions together with our preliminary results of NFS (Fe-57) experiments [25, 26], superconducting FeH_x phases can possibly be synthesized at pressures of about and above 150 GPa. At high pressures, we can also study the electronic and magnetic properties of FeH_x phases in NFS experiments, the crystal structure in X-ray diffraction (XRD) experiments, and the transport and magnetic properties in experiments on the measurement of the electrical resistance and the magnetic susceptibility.

In this work, iron polyhydrides are synthesized by the laser heating of samples in diamond anvil cells to temperatures of about 2000 K at pressures from 77 to 157 GPa. As a result, at least seven FeH_x compounds with different electronic and magnetic properties are synthesized. It is established that one of the polyhydride phases, which is identified as FeH_2, has the Néel temperature $T_N = 174$ K at a pressure of 82 GPa. One of the surprising results of this work is the detection of the FeH_x phase, which remains magnetically ordered at a pressure of 128 GPa in the temperature range of 4–300 K. Such a high pressure is characteristic of the boundary between the lower mantle and the outer core of the Earth.

2. EXPERIMENTAL METHOD

To synthesize iron polyhydrides in our experiments, we used a metallic iron powder enriched in the Mössbauer Fe-57 isotope to a degree of ~96%. The initial iron powder was pressed into plates about 0.5–2 μm thick with typical dimensions of 10 × 5 μm to 20 × 10 μm. Such a sample was placed in the working volume of a high-pressure diamond anvil cell, which was then filled with sublimated borazane (ammonia borane BH_3NH_3). Borazane served as a pressure-transmitting medium and simultaneously was a source of hydrogen at the laser heating of the sample (details of the synthesis method see in [3]). After that, the pressure in the cell was increased to the expected pressure of synthesis and the sample was heated by a laser. Borazane at a high temperature is decomposed stage-by-stage with the emission of atomic hydrogen as $NH_3BH_3 \rightarrow (NH_2BH_2)_n + H_2 \rightarrow (NHBH)n + H_2 \rightarrow$ c-BN + H_2 [27]. This hydrogen reacts with a metal at a high temperature and a high pressure and, as a result, higher FeH_x hydrides are synthesized.

The Mössbauer and X-ray diffraction measurements of iron hydrides at high pressures were performed in four diamond anvil cells (see Fig. 1) based on the ideas proposed in [28]. The working surface of diamond anvils 270–300 μm in diameter were beveled at an angle of 8.5° with the formation of a culet (flat area at the vertex of diamond) 40–55 μm in diameter.

Holes in the tungsten or rhenium gasket were laser drilled to approximately 35 and 400 μm in diameter. The c-BN powder mixed with a small amount of epoxy resin was pressed into a 400-μm hole in the metal gasket, and then the hole 35 μm in diameter was drilled in the c-BN gasket, which was the working volume. The inner c-BN gasket served as an insulating layer in the electrical resistance measurements.

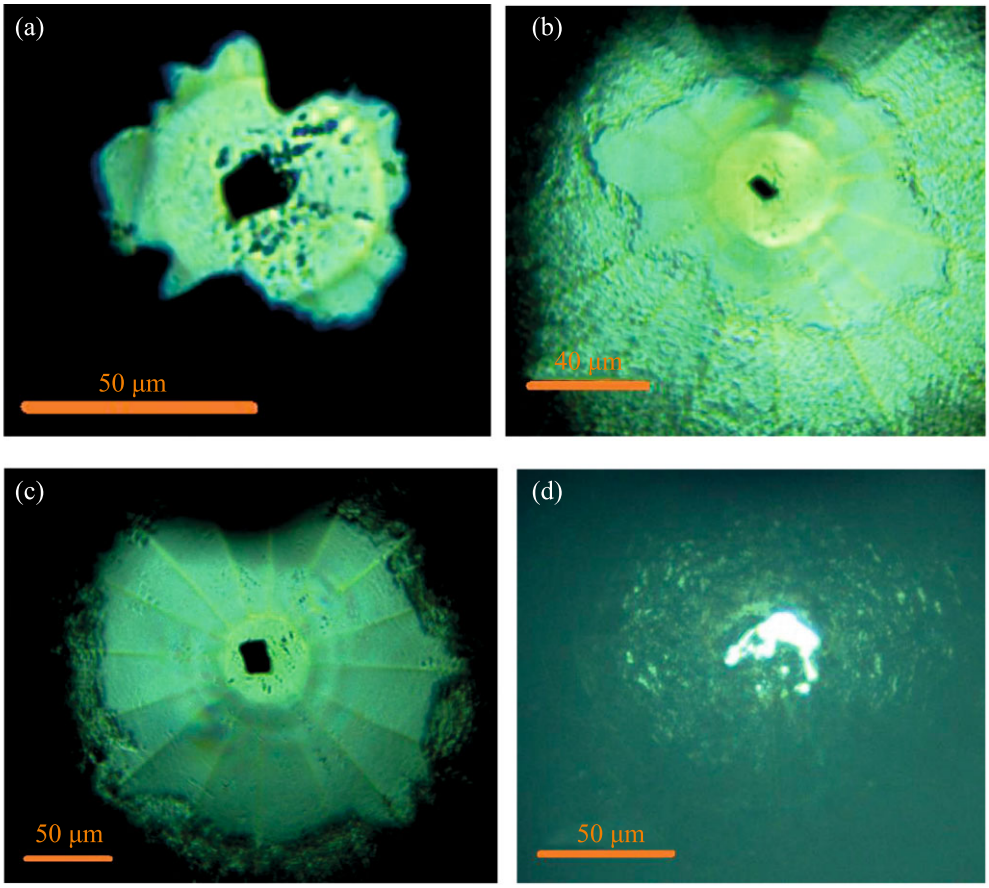

Fig. 1. (a) (Color online) Micrographs of samples loaded in four diamond anvil cells taken immediately after the synthesis of FeH_x polyhydride. The size of the working area of diamond anvils varies from 40 to 55 μm and the thickness of the FeH_x sample is about 0.5–2 μm. (a) Cell 1 with a W gasket; synthesis at a pressure of $P \sim 90$ GPa provided the I, Ia, and II phases; nuclear forward scattering was measured at pressures $P = 108-157$ GPa. (b) Cell 2 with a *c*-BN gasket, synthesis at a pressure of $P \sim 68$ GPa; diamond anvils were destroyed at a pressure of about 200 GPa. (c) Cell 3 with a *c*-BN gasket, synthesis at a pressure of $P \sim 154$ GPa gave the ε-Fe and III phases; nuclear forward scattering was measured at pressures $P = 110-156$ GPa. (d) TD-3 cell with a Re gasket, synthesis at a pressure of $P \sim 77$ GPa yields the IV(FeH_2), V, and VI phases; nuclear forward scattering was measured at $P = (82 \pm 2)$ GPa.

The pressure was determined using the diamond Raman scale [29]. Raman spectra were collected using a Raman spectrometer equipped with a 660-nm red laser, a Shamrock SR-500i-A monochromator, and a DU940N BV CCD detector.

It was found that the pressure gradient in the sample even at the maximum pressure in each cell was no higher than 5 GPa, which indicates a high degree of hydrostaticity of the borazane medium. Figure 1 shows micrographs of samples loaded in four DACs taken immediately after the synthesis of FeH_x polyhydrides.

Nuclear forward scattering spectra from Fe-57 nuclei in the synthesized FeH_x samples were recorded at the P01 beamline of the PETRA-III synchrotron (DESY, Hamburg, Germany) operating in the 40-bunch mode. We used a helium cryomagnetic system, where the high-pressure cells were cooled to temperatures of 3.8–4.3 K. The external magnetic field applied to the sample could be varied within 0–6 T. The characteristic acquisition rate of NFS spectra was about 150 photons/s, which allowed one to record high-quality NFS spectra each in 15–20 min. The system of KB mirrors focused the synchrotron beam into a 4 × 7-μm spot on the sample at a Mössbauer resonance energy of 14.41 keV.

The pressure in the cell was changed outside the cryostat at room temperature. Further, the cell was placed in the cryostat and was cooled to ~4 K. After that, several measurements of NFS spectra were performed under heating at different temperatures and in different magnetic fields in the range of 0–5 T. The magnetic field was parallel to the synchrotron beam, i.e., perpendicular to the plane of the sample. The pressure in the cell after the end of the heating cycle was additionally controlled at room temperature. The

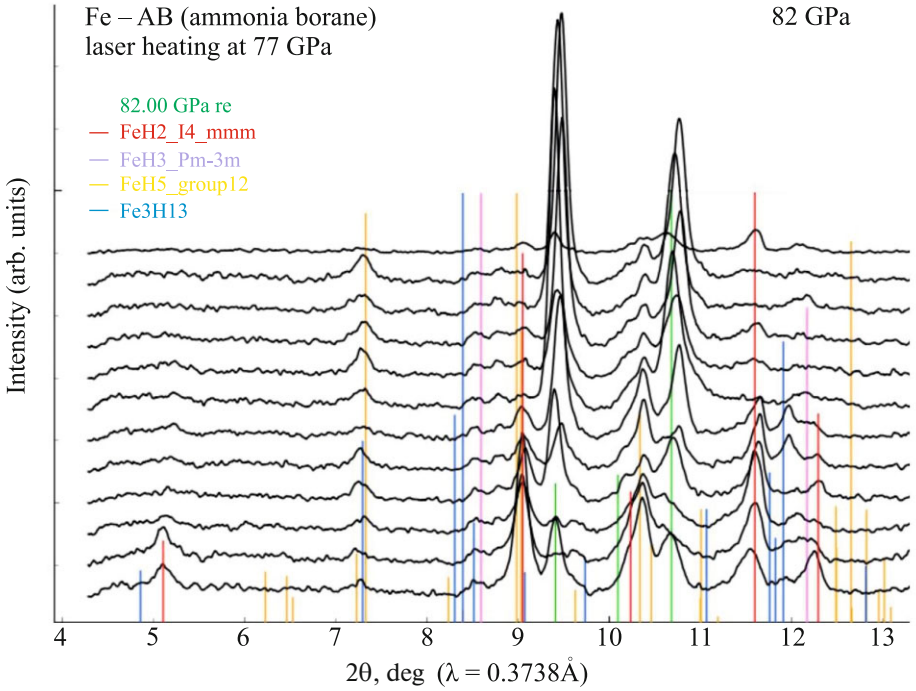

Fig. 2. (Color online) Synchrotron X-ray diffraction patterns recorded at 82 GPa during two-dimensional scanning of FeH_x synthesized in a TD-3 cell by laser heating the Fe sample in NH_3BH_3 medium.

stability of the pressure in the heating cycle was repeatedly tested and the deviations from the set value were no more than 5 GPa. The recorded NFS spectra were processed using the MOTIF library developed by Y.V. Shvyd'ko [30, 31].

Immediately after the NFS experiments, X-ray diffraction studies of the prepared samples were performed at the P02 beamline of the PETRA-III synchrotron (DESY, Hamburg, Germany) and at the ID27 beamline of the ESRF synchrotron (Grenoble, France). To determine the spatial distribution of phases in the sample, we used X-ray diffraction microscopy with a sharply focused intense X-ray beam with a diameter up to 3 μm at wavelengths of $\lambda = 0.289$ Å (P02, PETRA III) and $\lambda = 0.3738$ Å (ID27, ESRF). Two-dimensional scanning results in the recording of a set of X-ray diffraction patterns with a step of 2–5 μm, and after the X-ray diffraction analysis using the Dioptas [32] and XDI [33] programs, we reconstructed the two-dimensional distribution (map) of the identified microcrystalline phases.

3. EXPERIMENTAL RESULTS AND THEIR DISCUSSION

3.1. Measurement of X-Ray Diffraction and the X-Ray Diffraction Analysis of FeH_x Iron Polyhydrides at High Pressures

Figure 2 shows X-ray diffraction patterns recorded at the ID27 beamline of the ESRF synchrotron ($\lambda = 0.3738$ Å) from the region near the Re gasket (in the TD-3 cell), where several phases of iron hydrides could be present. Since the sample initially prepared for NFS measurements was a very thin layer with a thickness of about 0.5 μm, reflections in X-ray diffraction patterns have a low intensity insufficient to reliably determine crystalline phases. Reflections of the FeH_2 tetragonal hydride phase with the space group $I4/mmm$ (IV phase according to NFS data) are certainly detected, and additional weak reflections that can be due to the theoretically calculated FeH_3 (space group $Pm\text{-}3m$), FeH_5 (space group $C2/m$), and Fe_3H_{13} (space group $I4/mmm$) hydride phases are observed [11, 14]. Such a variety of different FeH_x structural phases indicates that the energies of these systems are very close to each other and requires a careful detailed analysis, recording the conditions of the synthesis, and the development of the conditions of the synthesis to ensure the reproducibility of the result.

Figures 3a and 4a show micrographs of the samples loaded in two diamond anvil cells. Figures 3b and 4b present the maps of the distribution of the dominant FeH_2 tetragonal phase. Figures 3c and 4c show the experimental X-ray diffraction pattern measured at the P02 beamline of the PETRA III synchrotron and the Le Bail full-profile refinement of the structural parameters of the FeH_2 phase at pressures of 82 and 117 GPa; the insets of Figs. 3c and 4c show the crystal

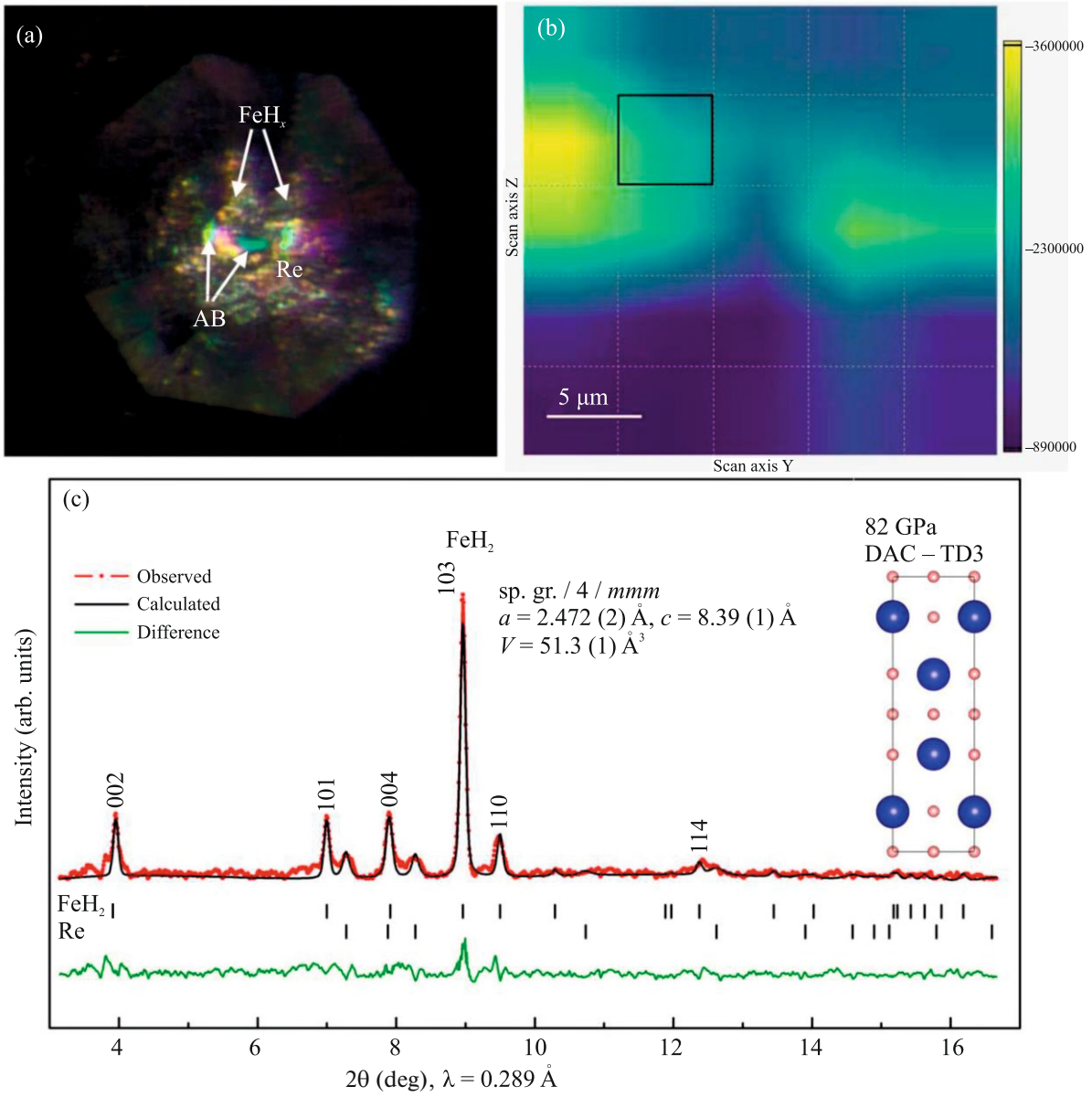

Fig. 3. (Color online) (a) Micrographs of the FeH_x sample synthesized by the laser heating of the Fe–NH_3BH_3 system at a pressure of 77 GPa in the TD-3 cell. (b) Distribution map of the FeH_2 phase in the sample at a pressure of 82 GPa. (c) X-ray diffraction pattern measured from the region marked in panel (b) and the Le Bail full-profile refinement of the structural parameters of FeH_2 at 82 GPa. The inset shows the crystal structure of FeH_2.

structure of FeH_2. The unit cell parameters of the tetragonal $I4/mmm$ FeH_2 phase at 117 GPa are found to be $a = 2.405(2)$ Å, $c = 8.17(1)$ Å, and $V = 47.3(1)$ Å^3.

3.2. Synthesis and NFS Studies of FeH_x Polyhydrides at Pressures of 77–157 GPa

Iron polyhydrides FeH_x were synthesized at high pressures and high temperatures using a laser heating setup at the P02 beamline of the PETRA-III synchrotron (DESY, Hamburg, Germany). The magnetic and electronic properties of FeH_x were studied by NFS (Fe-57) spectroscopy at high pressures at the beamline P01 of the PETRA-III synchrotron.

The time spectrum of nuclear resonance forward scattering from Fe-57 nuclei is the intensity of scattered synchrotron radiation as a function of the time after a synchrotron pulse. The decrease in nuclear excitation is modulated in time by quantum and dynamic beatings. Quantum beatings are due to the

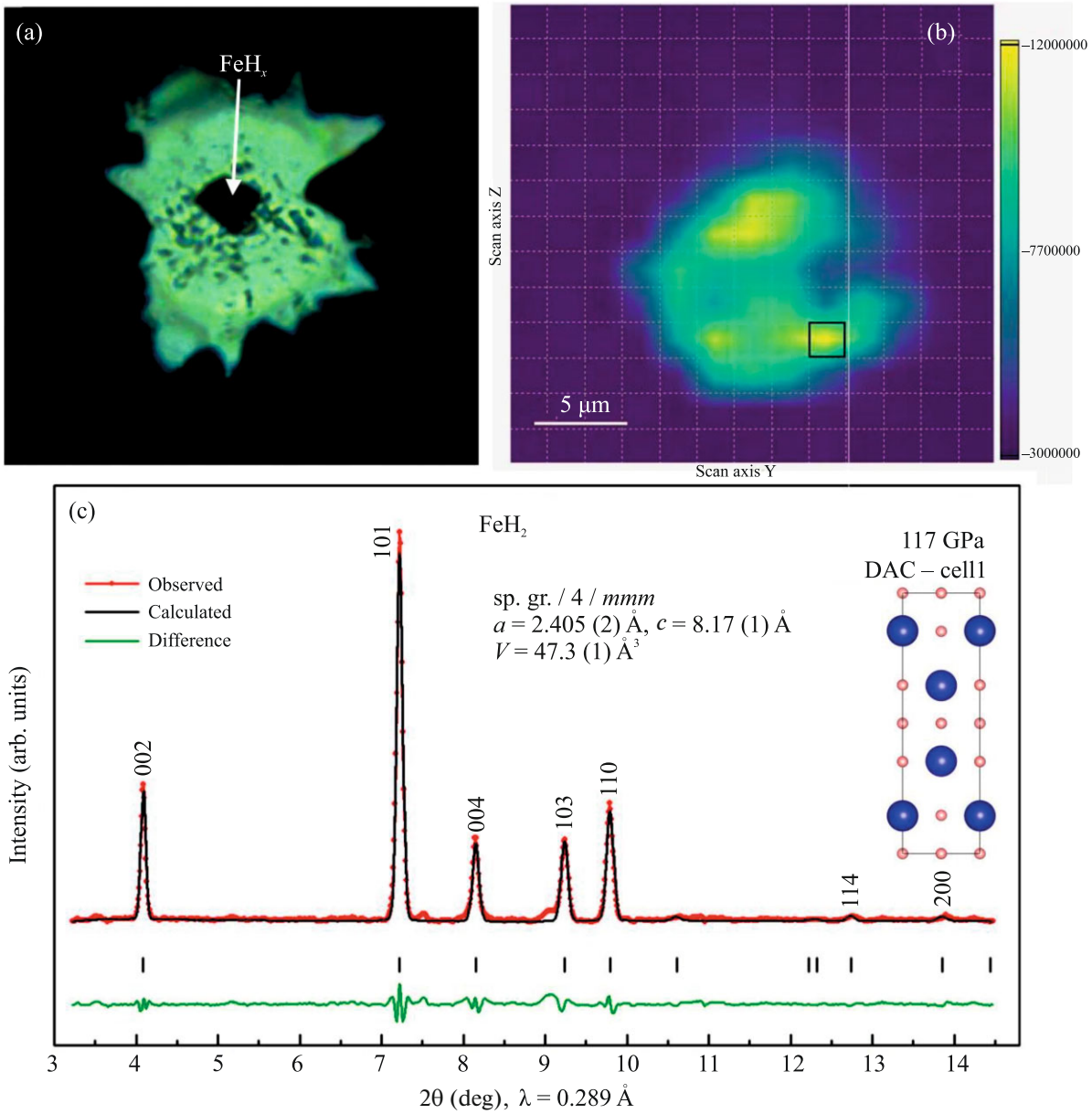

Fig. 4. (Color online) (a) Micrographs of the FeH_x sample synthesized by the laser heating of the Fe–NH_3BH_3 system at a pressure of 90 GPa in cell 1. (b) Distribution map of the FeH_2 phase in the sample at a pressure of 117 GPa. (c) X-ray diffraction pattern measured from the region marked in panel (b) and the Le Bail full-profile refinement of the structural parameters of FeH_2 at 117 GPa. The inset shows the crystal structure of FeH_2.

splitting of nuclear levels by the hyperfine interaction as a result of the interference between components of scattered radiation of sublevels with different frequencies. The period of quantum beatings is inversely proportional to the hyperfine splitting energy and, in our case, to the hyperfine magnetic field B_{hf} on iron nuclei (details see in [34]).

In the measured NFS spectra, we detected several different phases of FeH_x iron polyhydrides, where seven phases were established reliably. In this case, the I, Ia, and II phases after synthesis in cell 1 at a pressure of $P \sim 90$ GPa were further separated and studied. The ε-Fe and III phases were detected in the cell-3 at a synthesis pressure of $P \sim 154$ GPa. The IV(FeH_2), V, and VI phases were obtained in the TD-3 cell at a synthesis pressure of $P \sim 77$ GPa. Figure 5 shows seven NFS spectra characteristic of seven different FeH_x phases detected at the lowest temperature ~4 K in our experiment and from spectra recorded in the external magnetic field.

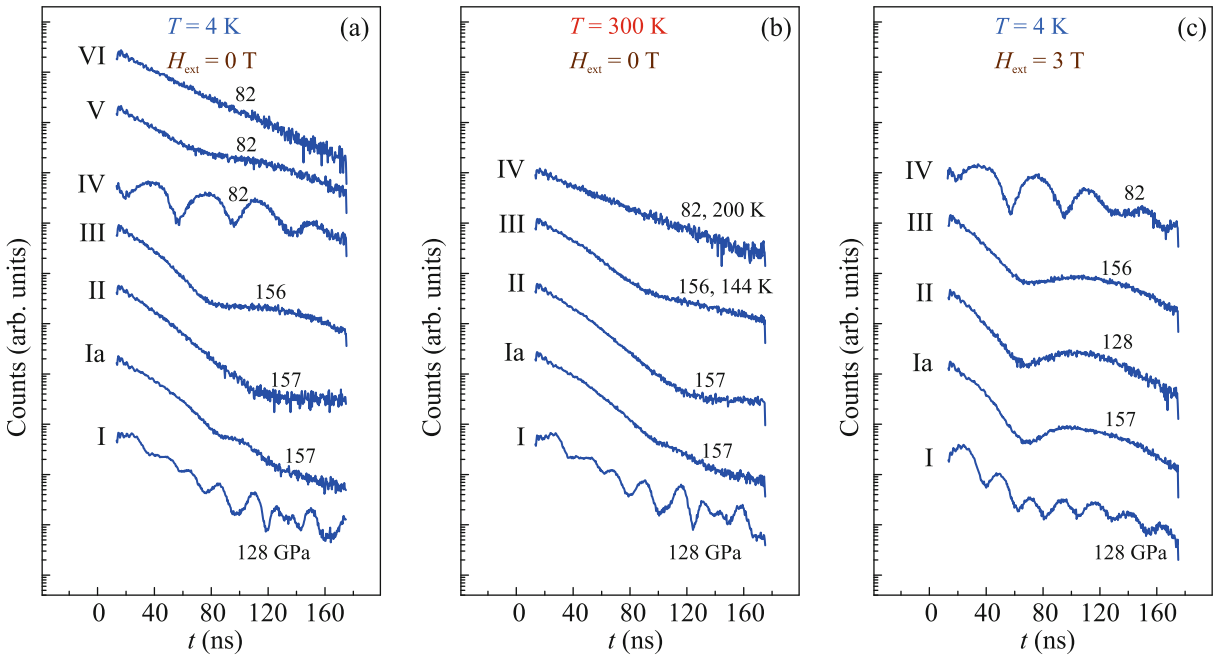

Fig. 5. (Color online) Examples of various FeH_x phases synthesized and studied at different pressures, temperatures, and magnetic fields: (a) at $T = 4$ K, (b) at room temperature and partially at temperatures much above 4 K, and (c) at $T = 4$ K in an external magnetic field of $H_{ext} = 3$ T.

The analysis of the dependence of NFS spectra on the temperature and external magnetic field H_{ext} indicates at least three antiferromagnetic phases (I, Ia, and IV, Figs. 5a–5c), two ferromagnetic phases (III and V) with a low magnetic moment (which is manifested in a low magnetic field on the iron nucleus B_{hf}), and two nonmagnetic phases (II and VI).

One of the surprising results of our experiment is the detection of the magnetic FeH_x (I) phase at a pressure of about 128 GPa and that this phase remains magnetic up to room temperature (see Fig. 5). This record high pressure at which a magnetically ordered iron compound has been detected to date corresponds to the pressure at the boundary between the lower mantle and the outer core of the Earth.

According to Figs. 5a and 5b, the I → Ia magnetic phase transition occurs in the pressure range of 128–140 GPa with an abrupt decrease in the magnetic moment at both low (4 K) and room temperatures. This transition is manifested in the drop of the hyperfine magnetic field B_{hf} on the iron nucleus by almost a factor of 4 in the NFS spectra! However, the Ia phase still remains weakly magnetic throughout the entire temperature range (4–300 K) at pressures up to ~156 GPa. The inverse Ia → I magnetic phase transition is not observed under the reduction of the pressure from 156 to 110 GPa in the I phase.

Thus, the I → Ia magnetic phase transition with the drop of the magnetic moment is likely a first-order structural phase transition with a large jump in the volume of the crystal lattice and a large hysteresis in the inverse Ia → I magnetic phase transition.

The effect of the temperature and the external magnetic field H_{ext} on the magnetic properties of the I phase was studied at a pressure of 128 GPa. Figure 6 shows the temperature evolution of NFS spectra of the I phase in an external magnetic field of H_{ext} = (a) 0 and (b) 1 T. Unlike the IV (FeH_2) phase, the I phase remains magnetic in the entire temperature range (4–300 K) at pressures at least up to 128 GPa with the average hyperfine magnetic field on the Fe-57 nucleus $B_{hf} \sim 20$ T.

The behavior of NFS spectra (Fig. 6) demonstrates that the hyperfine magnetic field B_{hf} in the I phase decreases slowly with increasing temperature from 4 to 300 K and decreases in the applied external magnetic field H_{ext}. This indicates the antiferromagnetic order. Nevertheless, the magnetic moment on iron remains high up to room temperature. A further investigation of the I phase is very important for understanding processes occurring at the boundary between the lower mantle and the core of the Earth.

Figure 7a shows the temperature evolution of NFS spectra in the IV phase. Analyzing the distribution of the phases over the area of the samples in X-ray diffraction and NFS experiments, we attribute this phase

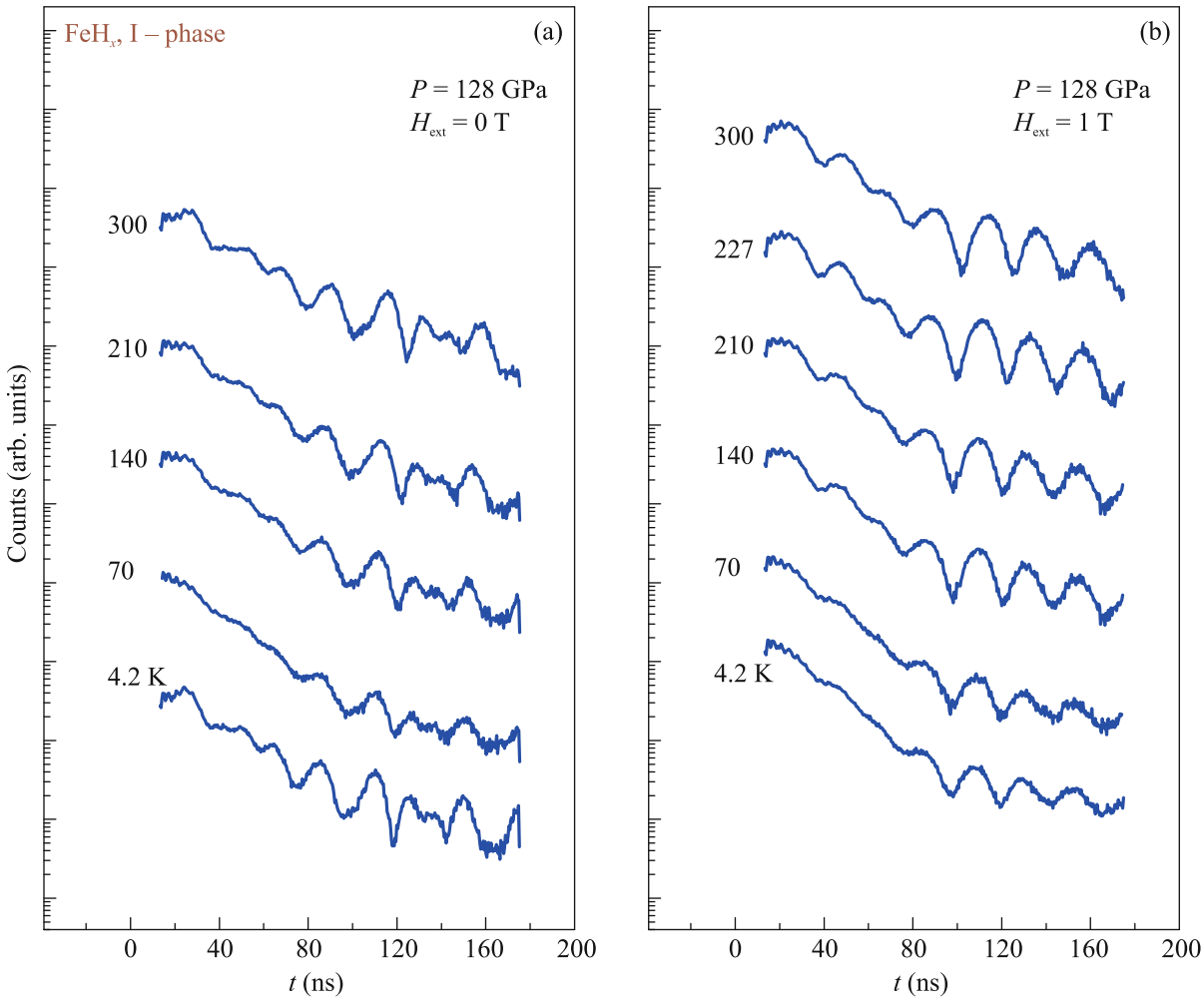

Fig. 6. (Color online) Temperature evolution of NFS spectra of the I phase in an external magnetic field of H_{ext} = (a) 0 and (b) 1 T at a pressure of 128 GPa.

to FeH_2 polyhydride. The hyperfine magnetic field B_{hf} at a pressure of 82 GPa decreases with increasing temperature, and the IV phase is transferred to a nonmagnetic state in the temperature range of 170–200 K. The Néel temperature at a pressure of 82 GPa is estimated at $T_N \sim 174$ K.

Figure 7b shows NFS spectra in the IV phase at a temperature of 4 K in an external magnetic field of H_{ext} = 0, 1, 3, and 5 T. It is established that the hyperfine magnetic field B_{hf} increases with the external magnetic field and jumps by a factor of almost 2 at H_{ext} = 5 T possibly because of the suppression of thermal spin fluctuations owing to the stabilization of the magnetic moment by the external magnetic field.

Using NFS spectra, we also examine the effect of the external magnetic field H_{ext} on the hyperfine magnetic field B_{hf} on the Fe-57 nucleus in pure iron prior to laser heating. Figure 8 presents NFS (Fe-57) spectra in pure iron at P = 110 GPa and T = 4 K in an external magnetic field of H_{ext} = 0, 1, 3, and 5 T parallel to the synchrotron beam, i.e., perpendicular to the plane of the sample. The inset shows the hyperfine field B_{hf} on the Fe-57 nucleus versus the external magnetic field H_{ext}. It is established that the magnetic field on iron nuclei at a temperature of 4 K coincides with the applied external magnetic field. This indicates that iron at a pressure of 110 GPa is nonmagnetic even at a temperature of 4 K (see the inset of Fig. 8).

These results together with NFS experiments on pure iron at various pressures and temperatures [25] allow one to use pure (nonmagnetic) iron as a sensor of an external magnetic field in experiments on the displacement of the magnetic field from the superconductor at high pressures just as the use of the Sn-119 Mössbauer sensor in experiments with the SH_3 superconductor in [2].

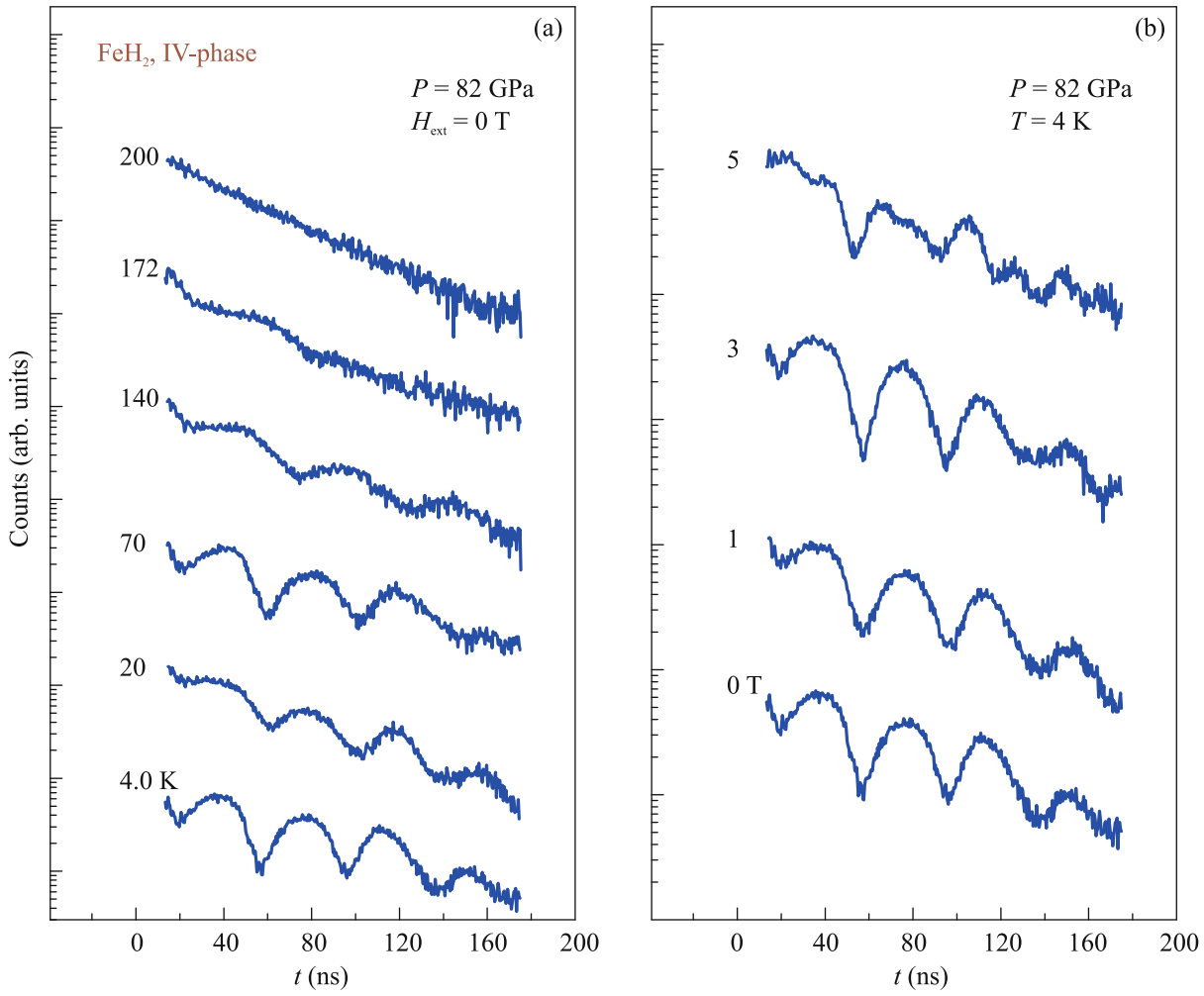

Fig. 7. (Color online) (a) Temperature evolution of NFS spectra in the IV phase at a pressure of $P = 82$ GPa; a transition to a nonmagnetic phase in the temperature range of ~172–200 K is established. (b) Nuclear forward scattering spectra in the IV phase at $T = 4$ K and a pressure of $P = 82$ GPa in an external magnetic field of $H_{ext} = 0$, 1, 3, and 5 T.

It is noteworthy that *nonmagnetic* FeH_x *phases* are very important to search for possible high-temperature superconductivity in iron polyhydrides. The FeH_x phase is very easily distinguished from pure iron in NFS spectra because they have strongly different isomer shifts. Figure 9 shows NFS spectra obtained at a pressure of 157 GPa from the nonmagnetic II phase synthesized in cell 1 at a pressure of $P \sim 90$ GPa in comparison with spectra from the ε-Fe phase. It is seen that measurements with an outer stainless steel (SS) reference make it possible to obtain different NFS spectra (see Fig. 9) and to study different phases independently. Furthermore, as discussed above, we analyzed the structures of these new phases with the X-ray diffraction of synchrotron radiation at the P02 beamline of the PETRA-III synchrotron (see Fig. 3) and at the ID-27 beamline of the ESRF synchrotron (see Fig. 2).

4. DISCUSSION OF THE RESULTS

Our experiments showed that a FeH_x polyhydride phase is very sensitive to the conditions of synthesis. Synthesis was initiated by heating of a part of the sample by 0.3-s intense laser pulses (wavelength of about 1 μm). The power of pulses was gradually increased until the appearance of visible luminescence of the sample. The estimated temperature of the heated sample is in the range of ~700–2000 K. Since the spot from the laser has a nonuniform intensity in the radial coordinate and it is smaller than the sample, heating leads to a large temperature gradient in the sample, which obviously results in the synthesis of different FeH_x phases. The synthesized phase depends apparently on the local thickness of the sample, on the power and duration of laser irradiation, and on the local temperature in the synthesis region. As a result, the synthesis region of a certain phase is characterized

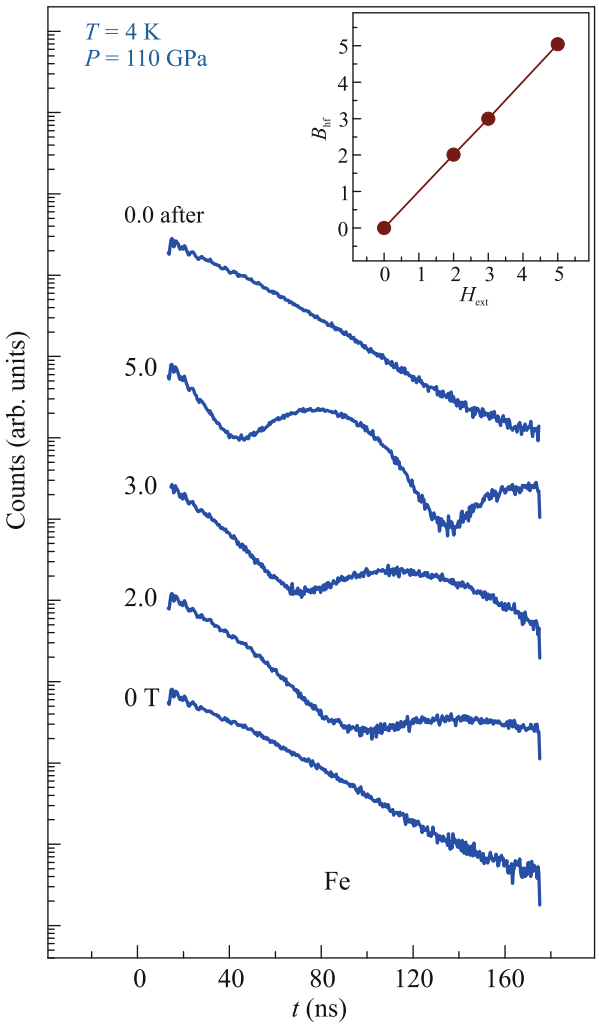

Fig. 8. (Color online) Nuclear forward scattering spectra in the pure nonmagnetic ε-Fe phase in an external magnetic field of H_{ext} = 0, 1, 3, and 5 T. The inset shows the hyperfine magnetic field B_{hf} on the Fe-57 nucleus versus the external magnetic field H_{ext} according to the calculation with the MOTIF library. The fields H_{ext} and B_{hf} are almost the same, indicating most probably that the ε-Fe phase is diamagnetic.

by a certain temperature and a certain hydrogen concentration formed during the decomposition of ammonia borane. The high pressure value also has an effect.

Thus, the nonuniform heating of the sample is useful for the synthesis of different FeH_x phases at the same pressure. If the sample is approximately twice as large as the laser spot, one phase is usually synthesized at a high temperature and the second phase is synthesized at a low temperature. This situation was, e.g., observed in cell 1, where the fundamentally different I, Ia, and II phases with strongly different magnetic properties were synthesized at a pressure of 90 GPa.

The performed experiments indicate that an entire sample should be uniformly heated with a small temperature gradient with the control of the maximum temperature of heating in order to obtain a uniform sample of one of several FeH_x phases.

Some synthesized FeH_x iron polyhydride phases were studied by synchrotron X-ray diffraction. The structural parameters of the tetragonal antiferromagnetic FeH_2 phase were determined. In addition, low-intensity X-ray diffraction peaks may indicate the possible presence of FeH_3, FeH_5, and Fe_3H_{13} hydrides.

According to NFS studies, there are several different FeH_x compounds with strongly different electronic and magnetic properties. One of the FeH_x phases is magnetic even at a high pressure up to at least 128 GPa, which is almost equal to the pressure at the boundary between the lower mantle and the outer core of the Earth. Several phases are antiferromagnetic (in particular, FeH_2), and several phases are nonmagnetic. Such a variety of FeH_x phases is due to very close energies of these systems and requires a careful detailed analysis and recording of the conditions of the synthesis.

Figure 10 shows the temperature dependence of the hyperfine magnetic field on the Fe-57 nucleus $B_{hf}(T)$ for the IV phase at a pressure of 82 GPa (TD2 cell). The hyperfine magnetic field B_{hf} was calculated from NFS spectra (see Fig. 7a) using the MOTIF library [30, 31]. According to the X-ray diffraction analysis (see Fig. 4), this phase at $P = 82$ GPa has the composition FeH_2 and a tetragonal structure with the space group $I4/mmm$.

The solid line in Fig. 10 is the approximation of the experimental points by the following empirical formula (critical coefficients), which we successfully used to describe the temperature dependence of the hyperfine magnetic field at various pressures [35, 36]:

$$B_{hf}(T) = B_0 \exp(-\alpha T/T_N)(1 - T/T_N)^{\beta}. \quad (1)$$

The best approximation is achieved with the parameters $T_N = 174$ K, $B_0 = 14.6$ T, $\alpha = 0.025$, and $\beta = 1/3$.

According to X-ray diffraction data, the II phase is also a tetragonal FeH_2 phase with the space group $I4/mmm$ (see Fig. 4), but it becomes nonmagnetic at pressures of 128 and 157 GPa throughout the entire temperature range of 4–300 K (see Fig. 5).

The I phase at a pressure of 128 GPa remains magnetic up to and possibly above room temperature (see Fig. 5). As mentioned above, this is of great geophysical interest because this pressure is close to that at the boundary between the lower mantle and the outer core of the Earth.

Using the data obtained (Fig. 6a), we plotted the temperature dependence of the hyperfine magnetic field $B_{hf}(T)$ on the Fe-57 nucleus for the I phase at a

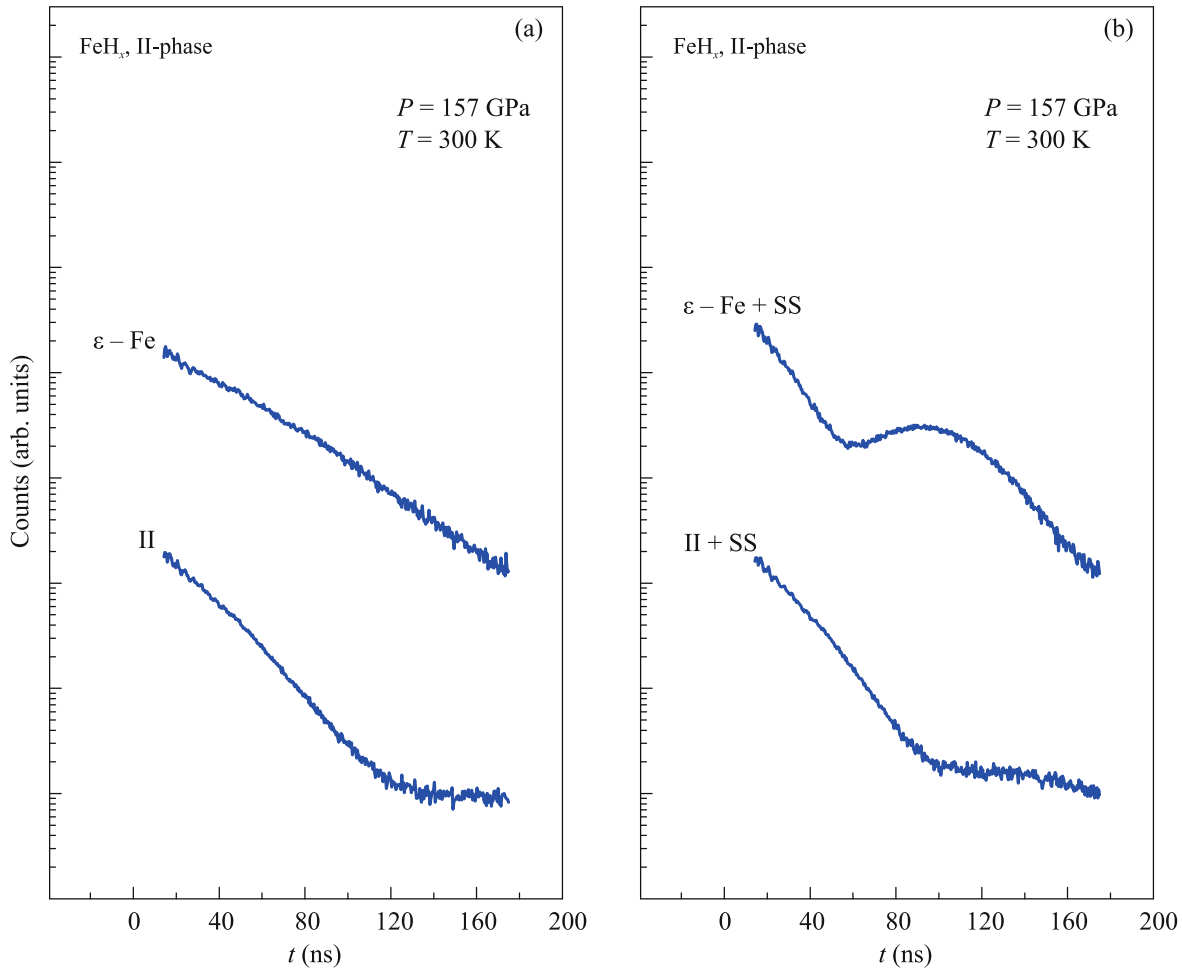

Fig. 9. (Color online) Example of the difference in the isomer shifts for pure iron and FeH_x hydride. Nuclear forward scattering spectra for (a) the II phase and pure iron and (b) the II phase with the external stainless steel reference (SS) and Fe + SS at T = 300 K and P = 157 GPa. A significant difference in the NFS spectra and the isomer shift is obvious.

pressure of 128 GPa (Fig. 11). The best approximation of the experimental points by the empirical formula (1) (solid line in Fig. 11) is achieved with the parameters T_N = 2100 K, B_0 = 21.4 T, α = 0.015, and β = 1/3. Thus, it can be expected that the FeH_x polyhydride I phase will be magnetic up to ~2000 K at a pressure of about 128 GPa. Unfortunately, the crystal structure of the IV phase was not reliably determined.

It is noteworthy that nonmagnetic polyhydride phases (FeH_x) are very important for the investigation of possible high-temperature superconductivity. These results are very important both fundamentally for the physics of metal polyhydrides and their magnetism and superconductivity and for the physics of the Earth and terrestrial magnetism.

We are planning further experiments in this field and theoretical analysis of the results.

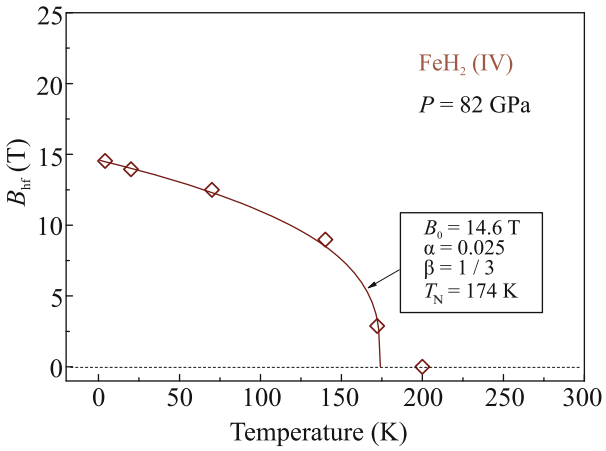

Fig. 10. (Color online) Temperature dependence of the hyperfine magnetic field B_{hf} on the Fe-57 nucleus for the FeH_2 (IV) polyhydride phase of a tetragonal structure with the space group $I4/mmm$ (TD2 cell) at a pressure of 82 GPa: experimental points fitted by (solid line) the function $B_{hf}(T) = B_0 \exp(-\alpha T/T_N)(1 - T/T_N)^{\beta}$ with the parameters T_N = 174 K, B_0 = 14.6 T, α = 0.025, and β = 1/3, which provide the best fit.

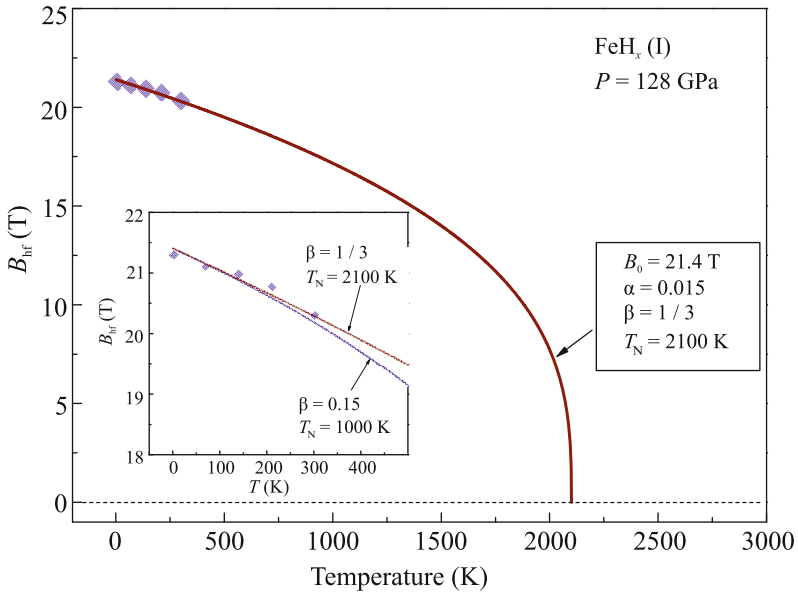

Fig. 11. (Color online) Temperature dependence of the hyperfine magnetic field B_{hf} on the Fe-57 nucleus for the FeH_x (I) phase at a pressure of 128 GPa: experimental points fitted by (solid line) the function $B_{hf}(T) = B_0 \exp(-\alpha T/T_N)(1 - T/T_N)^{\beta}$ with the parameters $T_N = 2100$ K, $B_0 = 21.4$ T, $\alpha = 0.015$, and $\beta = 1/3$. The inset shows experimental points fitted by the above function with the parameters (red line) $T_N = 2100$ K, $B_0 = 21.4$ T, $\alpha = 0.015$, and $\beta = 1/3$ and (blue line) $T_N = 1000$ K, $B_0 = 21.4$ T, $\alpha = 0.015$, and $\beta = 0.15$. It is seen that the former fit with $T_N = 2100$ K is better than the latter one with $T_N = 1000$ K.

ACKNOWLEDGMENTS

We are grateful to Olaf Leupold, Ilya Sergeev, and Hans-Christian Wille for the preparation of the NFS experiment and for assistance with the measurement of NFS spectra at the P01 beamline of the PETRA-III synchrotron (DESY, Hamburg, Germany); to Konstantin Glazyrin and Anna Pakhomova for assistance with the synthesis of polyhydrides in the laser heating device and with the measurement of X-ray diffraction patterns at the P02 beamline of the PETRA-III synchrotron (DESY, Hamburg, Germany); and to Piter Liermann for assistance with the measurement of the pressure at the Raman setup at the P02 beamline of the PETRA-III synchrotron (DESY, Hamburg, Germany).

FUNDING

This work was supported mainly by the Russian Science Foundation (project no. 21-12-00344). The adjustment system of the Raman installation was created under the support of the Ministry of Science and Higher Education (project no. 075-15-2021-1362). Facilities of the Center for Collective Use "Accelerator Center for Neutron Research of the Structure of Substance and Nuclear Medicine," of the Institute for Nuclear Research, Russian Academy of Sciences were used to load the samples. The preliminary X-ray studies were performed using the equipment of the Shared Research Center, Federal Scientific Research Centre Crystallography and Photonics, Russian Academy of Sciences and were supported by the Ministry of Science and Higher Education of the Russian Federation.

CONFLICT OF INTEREST

The authors declare that they have no conflicts of interest.

REFERENCES

1. A. P. Drozdov, M. I. Eremets, I. A. Troyan, V. Ksenofontov, and S. I. Shylin, Nature (London, U.K.) **525**, 73 (2015).
2. I. Troyan, A. Gavriliuk, R. Rüffer, A. Chumakov, A. Mironovich, I. Lyubutin, D. Perekalin, A. P. Drozdov, and M. I. Eremets, Science (Washington, DC, U. S.) **351**, 1303 (2016).
3. M. Somayazulu, M. Ahart, A. K. Mishra, Z. M. Geballe, M. Baldini, Y. Meng, V. V. Struzhkin, and R. J. Hemley, Phys. Rev. Lett. **122**, 027001 (2019).
4. I. A. Troyan, D. V. Semenok, A. G. Kvashnin, A. V. Sadakov, O. A. Sobolevskiy, V. M. Pudalov, A. G. Ivanova, V. B. Prakapenka, E. Greenberg, A. G. Gavriliuk, I. S. Lyubutin, V. V. Struzhkin, A. Bergara, I. Errea, R. Bianco, et al., Adv. Mater. **2006832**, 1 (2021).
5. D. Wang, Y. Ding, and H.-K. Mao, Materials **14**, 7563 (2021).
6. I. A. Troyan, D. V. Semenok, A. G. Ivanova, A. G. Kvashnin, D. Zhou, A. V. Sadakov, O. A. Sobolevskiy, V. M. Pudalov, I. S. Lyubutin, and A. R. Oganov, Phys. Usp. **65**, 748 (2022).
7. D. Y. Pushcharovsky, Geochem. Int. **57**, 941 (2019).
8. K. D. Litasov and A. F. Shatskiy, Russ. Geol. Geophys. **57**, 22 (2016).
9. Z. G. Bazhanova, V. V. Roizen, and A. R. Oganov, Phys. Usp. **60**, 1025 (2017).

10. K. D. Litasov, Z. I. Popov, P. N. Gavryushkin, S. G. Ovchinnikov, and A. S. Fedorov, Russ. Geol. Geophys. **56**, 164 (2015).
11. C. M. Pépin, A. Dewaele, G. Geneste, P. Loubeyre, and M. Mezouar, Phys. Rev. Lett. **113**, 265504 (2014).
12. C. M. Pépin, Science (Washington, DC, U. S.) **357**, 382 (2017).
13. Z. G. Bazhanova, A. R. Oganov, and O. Gianola, Phys. Usp. **55**, 489 (2012).
14. A. G. Kvashnin, I. A. Kruglov, D. V. Semenok, and A. R. Oganov, J. Phys. Chem. C **122**, 4731 (2018).
15. F. Li, D. Wang, H. Du, D. Zhou, Y. Ma, and Y. Liu, RSC Adv. **7**, 12570 (2017).
16. N. Zarifi, T. Bi, H. Liu, and E. Zurek, J. Phys. Chem. C **122**, 24262 (2018).
17. S. Zhang, J. Lin, Y. Wang, G. Yang, A. Bergara, and Y. Ma, J. Phys. Chem. C **122**, 12022 (2018).
18. D. N. Sagatova, P. N. Gavryushkin, N. E. Sagatov, I. V. Medrish, and K. D. Litasov, JETP Lett. **111**, 145 (2020).
19. A. Majumdar, J. S. Tse, M. Wu, and Y. Yao, Phys. Rev. B **96**, 201107(R) (2017).
20. C. Heil, G. B. Bachelet, and L. Boeri, Phys. Rev. B **97**, 214510 (2018).
21. E. C. Thompson, A. H. Davis, W. Bi, J. Zhao, E. E. Alp, D. Zhang, E. Greenberg, V. B. Prakapenka, and A. J. Campbell, Geochem. Geophys. Geosyst. **19**, 305 (2018).
22. J. V. Badding, R. J. Hemley, and H. K. Mao, Science (Washington, DC, U. S.) **253**, 421 (1991).
23. N. Hirao, T. Kondo, E. Ohtani, K. Takemura, and T. Kikegawa, Geophys. Res. Lett. **31**, L06616 (2004).
24. J. Ying, J. Zhao, W. Bi, E. E. Alp, Y. Xiao, P. Chow, G. Shen, and V. V. Struzhkin, Phys. Rev. B **101**, 020405(R) (2020).
25. A. Gavriliuk, I. Trojan, S. Aksenov, O. Leupold, I. Sergeev, H. Wille, A. Mironovich, I. Lyubutin, and V. Struzhkin, in *Proceedings of the EPSC-DPS Joint Meeting 2019* (2019), Vol. 13, p. EPSC-DPS2019-886.
26. I. S. Lyubutin, I. A. Troyan, and A. G. Gavrilyuk, in *Proceedings of the 16th International Conference on Mössbauer Spectroscopy and Its Applications* (2022), p. 68.
27. Yu. V. Kondrat'ev, A. V. Butlak, I. V. Kazakov, and A. Y. Timoshkin, Thermochim. Acta **622**, 64 (2015).
28. A. G. Gavriliuk, A. A. Mironovich, and V. V. Struzhkin, Rev. Sci. Instrum. **80**, 043906 (2009).
29. Y. Akahama and H. Kawamura, J. Appl. Phys. **100**, 043516 (2006).
30. Y. V. Shvyd'ko, Phys. Rev. B **59**, 9132 (1999).
31. Y. V. Shvyd'ko, Hyperfine Interact. **125**, 173 (2000).
32. C. Prescher and V. B. Prakapenka, High Press. Res. **35**, 223 (2015).
33. R. Hrubiak, J. S. Smith, and G. Shen, Rev. Sci. Instrum. **90**, 025109 (2019).
34. G. V. Smirnov, Hyperfine Interact. **123**, 31 (1999).
35. A. G. Gavriliuk, I. A. Trojan, I. S. Lyubutin, S. G. Ovchinnikov, and V. A. Sarkissian, J. Exp. Theor. Phys. **100**, 688 (2005).
36. A. G. Gavriliuk, I. S. Lyubutin, S. S. Starchikov, A. A. Mironovich, S. G. Ovchinnikov, I. A. Trojan, Y. Xiao, P. Chow, S. V. Sinogeikin, and V. V. Struzhkin, Appl. Phys. Lett. **103**, 162402 (2013).

Translated by R. Tyapaev